

Multivariate Boosted Trees and Applications to Forecasting and Control

L. Nespoli^a, V. Medici^a

^aISAAC, SUPSI Scuola Universitaria Professionale della Svizzera Italiana, Canobbio, CH

Abstract

Gradient boosted trees are competition-winning, general-purpose, non-parametric regressors, which exploit sequential model fitting and gradient descent to minimize a specific loss function. The most popular implementations are tailored to univariate regression and classification tasks, precluding the possibility of capturing multivariate target cross-correlations and applying conditional penalties to the predictions. In this paper, we present a computationally efficient algorithm for fitting multivariate boosted trees. We show that multivariate trees can outperform their univariate counterpart when the predictions are correlated. Furthermore, the algorithm allows to arbitrarily regularize the predictions, so that properties like smoothness, consistency and functional relations can be enforced. We present applications and numerical results related to forecasting and control.

1. Introduction

We propose the use of multivariate boosted trees (MBTs) to induce arbitrary regularization and consistency properties in the tree output. This can be done both via penalization of the multivariate output or requiring it to be a superposition of basis functions. Inducing regularization in multivariate output is not new, but while this is common for example in neural network architectures [1, 2, 3], they are currently not exploited in tree-based algorithms. One exception is the possibility of LightGBM and XGBoost to express monotonicity conditions of the univariate prediction, with respect to a given input [4]. This is obtained by inhibiting the tree growth if the new leaf causes a non-monotonic relationship in the selected feature. However, this may produce unnecessarily shallow trees if not enough split candidates are tested, which could be the case if the tree is grown using histogram search, one of the most popular methods for finding candidate splits.

2. Related work

In [5], an MGBT tailored to predicting longitudinal data is presented. This kind of data is typically generated in medical studies, sampling the population at different points in time. Typically, the amount of available data to model the temporal relation is limited. The authors developed MBTs and trained them in functional space, using B-Splines to model time interactions. The algorithm is tested on a synthetic dataset, generated using simple algebraic formulae to model the target dependence over features and time. In [6], a single tree is fitted using a multivariate linear regressor as weak learner. The

tree is grown such that in each leaf the dataset is divided into two classes, based on the points for which the tree returned an overshoot or undershot prediction. Despite the interesting idea, splitting points are not chosen with a variance reduction criterion, and only one model is fitted, thus not exploiting gradient boosting. The algorithm is found to perform better than linear regression on 3 machine learning datasets, while performance against LightGBM is datasets dependent. Recently, authors in [7] proposed a multivariate version of the XGBoost algorithm, introduced a new histogram algorithm for datasets with sparse features and implemented a performance tailored C++ library. In this work, we make use of the same approach to fit MBTs, coupling it with non-constant response functions.

2.1. Contributions

We have extended the formulation of boosted trees parameter space fitting to the multivariate and non-constant response cases. This goes beyond popular gradient boosting libraries, which adopt a univariate and constant response paradigm. To the best of our knowledge, no one has ever presented a non-constant response MBT. This new method allows us to arbitrarily regularize the covariance structure of the outputs, induce smoothness, consistency and functional relations, which are relevant properties for many applications.

In section 4.3, we introduce a smoothed formulation of the quantile loss and show its superiority in terms of modelling quantiles in the tails of the target distribution and crossings of the predicted quantile. A second linear-quadratic formulation of the quantile loss for trees is also introduced, and we show that its minimizers are the quantiles of the fitted distribution, independently from its shape. In section 4.2, we introduce a new approach for hierarchical forecasting, which takes into account previous forecast error, and show that this method is better compared to other state-of-the-art algorithms for the first prediction steps. This is possible thanks to the introduction of a consistent non-constant response function. Finally, in section 4.4, as

*This project is carried out within the frame of the Swiss Centre for Competence in Energy Research on the Future Swiss Electrical Infrastructure(SCCER-FURIES) with the financial support of the Swiss Innovation Agency(Innosuisse - SCCER program) and of the Swiss Federal Office of Energy(project SI/501523)

Nomenclature

Acronyms

cdf	cumulative density function
CV	cross validation
DDC	data driven control
GBT	gradient boosted tree
MAPE	mean absolute percentage error
MBT	multivariate boosted tree
MIMO	multiple-input multiple-output
MISO	multiple-input single-output
MPC	model predictive control
PCC	point of common coupling
pdf	probability density function
RMSE	root mean square error
VSC	voltage sensitivity coefficients

Variables and Functions

ϵ	prediction error
\hat{y}_b, \tilde{y}_b	forecasted and reconciled bottom time series
\hat{y}_u, \tilde{y}_u	forecasted and reconciled upper levels time series
$\mathbb{1}_x$	indicator function on condition x
\mathbb{E}	expectation operator
\mathcal{L}	loss function
$\bar{\chi}$	average number of quantile crossings
τ	quantile
\tilde{G}_k	$\sum_{i \in \mathcal{I}_l} \tilde{g}_{i,k}$
\tilde{g}_k	loss gradient w.r.t. w_k
\tilde{H}_k	$\sum_{i \in \mathcal{I}_l} \tilde{h}_{i,k}$
\tilde{h}_k	loss Hessian w.r.t. w_k
ε	boosted model training loss
F	boosted model
f	weak learner
$F_{Y x}$	cdf of random variable Y
g_k	loss gradient w.r.t. F_k

h_k	loss Hessian w.r.t. F_k
$k_{i,j}^p, k_{i,j}^q$	VSC for node i w.r.t. node j , for power and reactive power
p	probability
Q_s	quantile score
r	response function
r_τ	reliability of quantile τ
x	feature matrix
x_{lr}	feature matrix for linear response
y	target variable matrix

Parameters

Λ	quadratic punishment matrix
λ	quadratic punishment coefficient
\mathbb{I}_n	identity matrix of size n
Ω	error covariance matrix
ρ	learning rate
Θ	BT parameters
D	second order difference matrix
N	number of observations
n_b	number of bottom time series
n_f	features dimension
n_k	number of wavenumbers
n_l	number of leaves
n_r	number of boosting rounds
n_t	targets dimension
n_u	number of upper level time series
n_{min}	minimum number of observations per leaf
S	summation matrix
W	response function parameters
w_l	leaf-specific parameters

Sets

\mathcal{D}	dataset
\mathcal{I}_l	observations in leaf l
\mathcal{K}	set of wavenumbers

an example of application, we present a way to fit voltage sensitivity coefficients for electrical distribution networks through boosted trees, while retaining their theoretical linear formulation. The fit is based on few exogenous variables, and we show that robustness to input variable noise makes this approach suitable for control application.

3. Background

Given a matrix of targets $y \in \mathbb{R}^{N \times n_t}$, where N is the number of observations and n_t the dimensionality of the target, and a set of features (or covariates, or explanatory variables) $x \in \mathbb{R}^{N \times n_f}$, we call the union of their observations a dataset $\mathcal{D} = \{(x_i, y_i)_{i=1}^N\}$. Our goal is to fit a learnable model F on dataset \mathcal{D} , such that it minimizes the expected loss on unseen data, given a loss function $\mathcal{L}(y, F) : \mathbb{R}^{N \times n_t} \rightarrow \mathbb{R}$.

3.1. Decision trees

Since GBTs use trees as weak learners, we recall here their formal description and fitting strategy. A tree can be described as:

$$f(x_i, \Theta) = \sum_{l=1}^{n_l} r(w_l) \mathbb{1}_l(x_i) \quad (1)$$

where n_l is the number of subspaces (leaves) into which the feature space has been partitioned, $\mathbb{1}_l(x_i) : \mathbb{R}^{n_f} \rightarrow \{0, 1\}$ is an indicator function returning 1 if x_i belongs to the l_{th} leaf, and $r(w_l)$ is a response (or basis) function, parametrized by some leaf-specific coefficients w_l . Here $\Theta = \{S, W\}$ consists of both the set of variables defining the splits S and the parameter set of the response functions W . While in this paper we will make use of different response functions, in the standard case this is a constant, thus $r_l = w_l$, where $w_l \in \mathbb{R}^{n_t}$, and $n_l = 1$ corresponds to the univariate case. Usually, the partition function $\mathbb{1}_l$ is obtained by binary splits on a given feature, and as such, leaves are orthogonal and disjoint subspaces of the feature space. In order to fit both mono and multivariate trees, we can rely on the following remark:

Remark 1. *Since the functional form $r(w_l)$ is the same for each leaf, w_l is constant for a given leaf, and since the leaves are disjoint subspaces of the feature space, we only need to know the functional form of the leaves' loss function in order to fit a tree.*

We can then write the total loss, as a summation of the leaf losses:

$$\begin{aligned} \mathcal{L}(y, f(x, \Theta)) &= \sum_{i=1}^N \mathcal{L}(y_i, f(x_i, \Theta)) \\ &= \sum_{i=1}^N \mathcal{L}\left(y_i, \sum_{l=1}^{n_l} r(w_l) \mathbb{1}_l(x_i)\right) \\ &= \sum_{l=1}^{n_l} \sum_{i \in \mathcal{I}_l} \mathcal{L}(y_i, r(w_l)) = \sum_{l=1}^{n_l} \mathcal{L}_l \end{aligned} \quad (2)$$

where $\mathcal{I}_l = \{i : \mathbb{1}_l(x_i) = 1\}$. To fit the tree, we must find both the optimal values of w_l inside a given leaf, and the leaf partitions \mathcal{I}_l . While the first task is straightforward, the second one is much harder; in fact, since the latter is usually computationally infeasible, greedy algorithms are used to find the best splits. Basically, at each iteration, a leaf with dataset \mathcal{D}_l is split if the sum of the loss computed on the partial datasets $\mathcal{D}_{l,s1}$ and $\mathcal{D}_{l,s2}$ is lower than the leaf loss. It is easy to see that the splitting criterion (that is, how to divide \mathcal{D}_l), must be only dependent on the features x since at prediction time we won't know the values of y . Even if this approach is simple, it can result in high computational costs; in the extreme case in which all the points are regarded as splitting candidates, the computational cost of the algorithm is $\mathcal{O}(N \times n_f)$ for the first splitting decision. In this paper, we restrict splitting candidates using histograms, as done in LightGBM [8]. This reduces the cost of finding the optimal split to $\mathcal{O}(n_b \times n_f)$ where n_b is the number of considered bins.

3.2. Boosted trees

Boosting algorithms have progressively gained popularity among the machine learning and statistics community, starting from the introduction in the 90s of the famous AdaBoost classification algorithm [9]. Originally introduced as an ensemble method [10], boosting was later interpreted as a gradient descent in functional space [11], opening up the possibility of using it for optimizing a wide variety of smooth and non-smooth objective functions. In this paper, we follow the interpretation of boosting as an iterative optimization strategy for statistical learning. In this section, we review the original gradient descent interpretation in functional space presented in [12] and the optimization in parameter space using second order approximations adopted by more recent algorithms.

For a give model F , under the hypothesis that $\mathcal{L}(y, F)$ is continuous and smooth almost everywhere, we can seek its minimizer F^* through gradient descent iterations. To simplify the notation, we refer to $\frac{\partial \mathcal{L}(y, F_k)}{\partial F_k}$ as g_k , that is, the gradient of the loss function with respect to the model at iteration k . As it is known, this is equivalent to solve the following minimization problem at each iteration k :

$$F_{k+1} = \underset{F}{\operatorname{argmin}} \mathcal{L}(y, F_k) + g_k(F - F_k) + \frac{1}{2\rho}(F - F_k)^2 \quad (3)$$

where ρ is a parameter. Equation (3) can be interpreted as the act of minimizing the first order approximation of the loss function in its argument F , while trying not to deviate too much from the previous fitted model F_k . In order to find the minimizer of (3), we apply the first order optimality condition and find:

$$F_{k+1} = F_k - \rho g_k \quad (4)$$

which is the gradient descent step. The loss gradient g_k is easily computed for the dataset \mathcal{D} . However, as pointed out in [12], our goal is to minimize $\mathcal{L}(y, F)$ not only for the dataset \mathcal{D} , but also on unseen data, in order to perform statistical learning and achieve model generalization. For this reason, boosting in functional space uses the gradient *learned* by a base model $f(x, \Theta)$,

also known as weak learner, where Θ is the set of the model's parameters. The iterative model fitting becomes:

$$F_{k+1} = F_k - \rho f_k \quad (5)$$

where $f_k(x, \Theta)$ has been fitted under least squares criterion on g_k . Boosting in functional space is a building block of many other machine learning algorithms. For example, it has been recently adopted, in combination with parametric probabilistic modelling and the concept of natural gradient, in the NGBoost library [13]. In this paper, we will follow the method adopted by XGboost and LightGBM, which optimizes the boosted tree in parameter space using a second-order approximation of the loss function. We retain only the additive stage-wise strategy defined by the iteration (5), assuming it to be coercive with respect to the prediction error. Indeed the presence of ρ helps in dumping the response of the current iteration model, avoiding overshooting of the final model F_{k+1} . Defining $y_k = y - F_k$, we have:

$$f_{k+1} = \underset{\Theta}{\operatorname{argmin}} \mathcal{L}(y_k, f_k) + \tilde{g}_k f(\Theta) + \frac{1}{2} \tilde{h}_k f(\Theta)^2 + \lambda w_l^2 \quad (6)$$

where λ is the quadratic punishment coefficient, \tilde{g} and \tilde{h} are the gradient and the second derivative of the loss function, with respect to the model *parameters*. For the chain rule, we can write:

$$\tilde{g} = g \frac{\partial r(w_l)}{\partial w_l} \quad \tilde{h} = g \frac{\partial^2 r(w_l)}{\partial w_l^2} + h \left(\frac{\partial r(w_l)}{\partial w_l} \right)^2 \quad (7)$$

where $h = \frac{\partial^2 \mathcal{L}}{\partial F^2}$ and $r(w_l)$ is the tree response function, introduced in (1). Note that for the usual case in which the leaf response is constant, $\tilde{g} = g$ and $\tilde{h} = h$. In order to minimize (6), we apply the two-step strategy explained in section 3.1. At first, the optimal leaf loss given the splits $\{\mathbb{I}_l\}_1^n$ is retrieved, and secondly, a greedy strategy is applied to find the optimal splits. The overall loss function (disregarding the constant term) can be now defined using (2):

$$\mathcal{L}(y, f_k) \simeq \sum_{l=1}^{n_l} \lambda w_l^2 + \sum_{i \in \mathcal{I}_l} \tilde{g}_k w_l + \frac{1}{2} \tilde{h}_k w_l^2 \quad (8)$$

Thus, for the l_{th} leaf, the optimal w_l given the split is:

$$w_l^* = \frac{-\sum_{i \in \mathcal{I}_l} \tilde{g}_{i,k}}{\lambda + \sum_{i \in \mathcal{I}_l} \tilde{h}_{i,k}} \quad (9)$$

The optimal leaf loss becomes:

$$\mathcal{L}_l^* = -\frac{1}{2} \frac{\sum_{i \in \mathcal{I}_l} \tilde{g}_{i,k}^2}{\lambda + \sum_{i \in \mathcal{I}_l} \tilde{h}_{i,k}} \quad (10)$$

Since we kept the same procedure for fitting univariate boosted trees in the multivariate case, we postpone the presentation of the detailed fitting procedure in the next section.

3.3. MBTs

Multivariate GBTs can be fitted by following the same procedure described in the previous section. The only difference relies on the dimensionality of the target variable $y \in \mathbb{R}^{N \times n_t}$ where n_t is strictly greater than 1. The second derivative in equation (8) is replaced by the Hessian of the loss function $\mathcal{L}(y, f_k)$. For clarity, we report the matrix form of \tilde{g} and \tilde{h} in the multivariate case, for which (7) are the univariate analogous:

$$\tilde{g} = g \left(\frac{\partial r(w_l)}{\partial w_l} \right) \quad (11)$$

$$\tilde{h} = g \frac{\partial^2 r(w_l)}{\partial w_l^2} + \frac{\partial r(w_l)}{\partial w_l}^T h \frac{\partial r(w_l)}{\partial w_l} \quad (12)$$

where $g \in \mathbb{R}^{N \times n_t}$, $h \in \mathbb{R}^{n_t \times n_t}$, $\frac{\partial r(w_l)}{\partial w_l} \in \mathbb{R}^{n_t \times n_r}$, $\frac{\partial^2 r(w_l)}{\partial w_l^2} \in \mathbb{R}^{n_t \times n_r \times n_r}$. Note that the number of dimensions of the leaf parameter vector, n_r , may be different from the dimensionality of the target, n_t . For example, this is the case of hierarchical forecasting, presented in section 4.2. We stress out that in the multivariate case, the second derivative of the response function is a 3-order tensor. However, as we will see, for many combinations of objective function and responses, MBT fitting won't require to store or compute the whole tensor, considerably simplifying the computational effort. For the sake of notation, replacing $\sum_{i \in \mathcal{I}_l} \tilde{g}_{i,k}$ with \tilde{G} and $\sum_{i \in \mathcal{I}_l} \tilde{h}_{i,k}$ with \tilde{H} , the optimal response (9) and the optimal loss (10) can be rewritten as:

$$w_l^* = (\Lambda + \tilde{H})^{-1} \tilde{G} \quad (13)$$

$$\mathcal{L}_l^* = \tilde{G}^T (\Lambda + \tilde{H})^{-1} \tilde{G} \quad (14)$$

where $\Lambda \in \mathbb{R}^{n_r \times n_r}$ is the quadratic punishment matrix, which weights the L2 norm penalization of the model parameters, $\|w_l\|_\Lambda^2$. The complete procedure for fitting the MBT is described in algorithm 2 and 1. Algorithm 1 describes the boosting procedure: starting from an initial guess for \hat{y} , which in this case corresponds to the column-expectations of y , we retrieve the gradient \tilde{g} and hessian matrices \tilde{h} for all the observations of the dataset (line 3), given the loss function \mathcal{L} and the leaf response function r . At line 4 the weak learner at iteration k is fitted using the `fit-tree` algorithm described in 2. Then the overall model F_k is updated (line 5) along with the training loss (line 6). This is computed through the exact formulation of the loss function and includes a term for the penalization of the number of leaves T in the final model F_k :

$$\varepsilon = \mathcal{L}(y, F_k(x)) + \rho T \quad (15)$$

The procedure ends if the training loss is not decreasing or the iterations exceeded the maximum number n_r . Algorithm 2 describes the recursive procedure to fit the multivariate tree. At line 1-2 the algorithm halts if the number of observations is lower than a threshold, n_{min} . If this is not the case, the total leaf loss is computed (line 3), and the best split point search is carried out for all the variables in x (line 4). As anticipated, we use the same histogram search adopted in XGboost and LightGBT, see algorithm 2 in [14] and algorithm 1 in [8]. Briefly

speaking, instead of enumerating all the possible split points as done by the pre-sorting algorithm [15], only a few numbers of quantiles are tested for each feature. This does not reduce too much the final regressor accuracy; on the other hand, since finding the best split takes most of the computational time of boosted tree algorithms, this procedure substantially speeds up the fitting process. At line 5, the quantiles for the j_{th} feature are retrieved and are then used at line 7 to obtain the partial sums of the gradient and Hessian, based on the split point q and variable j . The split-loss $\mathcal{L}_a + \mathcal{L}_b$ is then computed using equation (14); if this value is lower than the current minimum, the latter and the best split candidate are updated (line 10-11). Finally, if a split with a total loss lower than \mathcal{L}_0 has been found, the procedure is called recursively, with partial datasets, gradients and Hessian, based on the best split. Otherwise, the current node is considered a terminal leaf, and the optimal response is computed based on equation (13).

Algorithm 1: MGBT training

Input: training dataset: $\mathcal{D}_{tr} = \{(x_i, y_i)_{i=1}^N\}, \mathcal{L}, r, n_r$
Output: boosted tree F

```

1  $\hat{y} \leftarrow [\mathbb{E}_j y_{ji}]_{i=1}^{n_r}$  ▷ initial guess
2 while  $k < n_r$  and  $\varepsilon < \varepsilon_{k-1}, k++$  do
3    $\tilde{g}, \tilde{h} \leftarrow \hat{y}, y, \mathcal{L}, r$ 
4    $f_k \leftarrow \text{fit-tree}(x, y, \tilde{g}, \tilde{h})$ 
5    $F_k \leftarrow F_{k-1}, f_k$ 
6    $\hat{y}, \varepsilon \leftarrow F_k, x, y$ 
7    $\varepsilon_{k-1} \leftarrow \varepsilon_k$ 

```

Algorithm 2: fit-tree

Input: $x, y, \tilde{g}, \tilde{h}, f, node$
Output: tree f

```

1 if  $\text{length}(x) < n_{min}$  then
2   return
3  $\mathcal{L}_0 = \mathcal{L}^* \leftarrow G, H$ 
4 for  $x_j \in x^T$  do ▷ find best split
5    $q_j \leftarrow x_j, n_q$ 
6   for  $q \in q_j$  do ▷ histogram search
7      $\tilde{G}_a, \tilde{H}_a, \tilde{G}_b, \tilde{H}_b \leftarrow \tilde{g}, \tilde{h}, q, j$ 
8      $\mathcal{L}_a, \mathcal{L}_b \leftarrow \tilde{G}_a, \tilde{H}_a, \tilde{G}_b, \tilde{H}_b$ 
9     if  $\mathcal{L}_a + \mathcal{L}_b < \mathcal{L}^*$  then
10       $f[node].split \leftarrow (q, j)$ 
11       $\mathcal{L}^* \leftarrow \mathcal{L}_a + \mathcal{L}_b$ 
12 if  $\mathcal{L}_0 < \mathcal{L}^*$  then ▷ recursive split
13    $\tilde{g}_a, \tilde{h}_a, \tilde{g}_b, \tilde{h}_b \leftarrow \tilde{g}, \tilde{h}, f[node].split$ 
14    $x_a, y_a, x_b, y_b \leftarrow x, y, f[node].split$ 
15    $\text{fit-tree}(x_a, y_a, \tilde{g}_a, \tilde{h}_a, f, node_a)$ 
16    $\text{fit-tree}(x_b, y_b, \tilde{g}_b, \tilde{h}_b, f, node_b)$ 
17 else ▷ compute best response
18    $f[node].r_{opt} \leftarrow r((\tilde{H} + \Lambda)^{-1} \tilde{G})$ 

```

4. Multivariate Regularization

In this section, we introduce some of the most relevant loss functions and multivariate responses that can be modelled through the proposed MBT.

4.1. Covariance structure and Smoothing

Generally speaking, imposing a learning bias on the covariance structure of the target can be beneficial for any machine learning algorithm. The most known example of this is linear regression fitting under generalized least squares; in this case, the estimated covariance matrix of the errors $\hat{\Omega}$ is used to penalize the model's errors differently. This can be readily integrated using a linear response function (as explained in section 4.2). Under a constant model response, $r(w_l) = w_l$, the covariance structure of the data can be taken into account by means of the quadratic punishment matrix Λ . For example, we can impose a given smoothness of the response using a filtering approach [16] such as an Hodrick-Prescott filter [17], punishing the discrete second-order derivative of r . This can be obtained setting $\Lambda = \lambda D^T D$ where $D \in \mathbb{R}^{(n_r-2) \times n_r}$ is the second-order difference matrix:

$$D = \begin{bmatrix} 1 & -2 & 1 & & & \\ & & \ddots & \ddots & \ddots & \\ & & & 1 & -2 & 1 \\ & & & & 1 & -2 & 1 \end{bmatrix} \quad (16)$$

Since under constant response $h = \mathbb{I}_{n_t}$ where \mathbb{I}_{n_t} is the identity matrix of dimension n_t , we have:

$$\Lambda + H = \lambda D^T D + n_t \mathbb{I}_{n_t} \quad (17)$$

where n_t is the number of observations in the current leaf. The previous expression can be replaced in (13) and (14) to retrieve the optimal response and loss of MBT, respectively.

Imposing a condition on the derivative smoothness of the response can be seen as a way to perform signal denoising. If the Hodrick-Prescott filter is applied in a forecasting task, the approach becomes similar to denoising the time series with an a priori smoothing. However, imposing smoothness of the forecasted signal gives the regressor a chance to predict statistically significant peaks, that would have been smoothed out in the pre-processing phase.

A second approach to induce prediction regularization is through smoothing via basis function [18]. As recently proposed in [1] in the context of forecasting with neural networks, we can couple a Fourier expansion with the MBT algorithm. We define the response as $r = Pw$ where $P \in \mathbb{R}^{n_t \times 2n_k}$ is a projection matrix onto sine and cosine functional space with n_k different wavenumbers:

$$P = \left[\begin{bmatrix} \cos\left(k \frac{2\pi t}{n_t}\right)^T, \sin\left(k \frac{2\pi t}{n_t}\right)^T \end{bmatrix}^T \right]_{k \in \mathcal{K}} \quad (18)$$

where $t = [1, 2, \dots, n_t]$ and \mathcal{K} is the set of considered wave numbers. Under L2 loss, the i_{th} component of the loss function

gradient and Hessian can be written as:

$$\tilde{g}_i = -P^T g_i \quad (19)$$

$$\tilde{h}_i = P^T P = \mathbb{I}_{n_r} \quad (20)$$

where the last equality holds due to the fact that P is orthonormal. Under these conditions (13) then becomes:

$$w_l^* = -(\Lambda + n_l \mathbb{I}_{n_r})^{-1} P^T G \quad (21)$$

where $G = \sum_{i \in \mathcal{I}_l} g_i$, and (14) becomes:

$$\mathcal{L}_l^* = G^T P (\Lambda + n_l \mathbb{I}_{n_r})^{-1} P^T G = G^T (\Lambda + n_l \mathbb{I}_{n_r})^{-1} G \quad (22)$$

where the last equality holds again for the orthonormality of P , and Λ being diagonal.

4.2. Latent variables and hierarchical forecasting

In several applications, we are interested in responses that are linear combinations of a fixed matrix $S \in \mathbb{R}^{n_r \times n_r}$. That is, S is kept constant through leaves and boosting rounds, while the response $r = S w_l$ can change conditionally to the observations. This procedure restricts the response to lie in the span of S . When the dimensionality of w_l is smaller than the response ($n_r < n_t$), w_l can be seen as latent variables generating the full response. Latent variables are usually used to induce regularization in regression [19]. Loosely speaking, it is easy to see that all the (conditional) information which is needed to generate $y \in \mathbb{R}^{N \times n_t}$ is already presented in $x \in \mathbb{R}^{N \times n_r}$ if $y^T = C x^T + \varepsilon$, where $C \in \mathbb{R}^{n_r \times n_t}$ is constant. A notable application of this approach is hierarchical forecasting: a method to correct forecasts of hierarchically structured signals, which increases the overall forecasting accuracy, by ensuring that the corrected forecasts are consistent under addition. If we define the bottom time series forecasts as $\hat{y}_b \in \mathbb{R}^{T \times n_b}$, the one generated by aggregations as $\hat{y}_u \in \mathbb{R}^{T \times n_u}$, the whole set of original forecasts is then denoted as $\hat{y} = [\hat{y}_u^T, \hat{y}_b^T]^T \in \mathbb{R}^{T \times n_t}$, where $n_t = n_b + n_u$ and n_b and n_u are the number of the bottom and upper time series. Hierarchical forecasting consists in finding a set of corrected bottom forecasts, \tilde{y}_b , which minimize the overall forecast error and such that the following equation holds:

$$\tilde{y}^T = S \tilde{y}_b^T \quad (23)$$

where \tilde{y} are the corrected signals for the whole hierarchy and $S \in \mathbb{R}^{n \times n_b}$ is a summation matrix. An example of a three-level summation matrix is the following:

$$S = \begin{bmatrix} 1 & 1 & 1 & 1 \\ 1 & 1 & 0 & 0 \\ 0 & 0 & 1 & 1 \\ & & & \mathbb{I}_4 \end{bmatrix} \quad (24)$$

In [20], the authors used ordinary least squares regression to reconcile the forecasts in the hierarchy. Elaborating on this approach, [21, 22] proposed a trace minimization method (called minT) in which the covariance matrix of the forecasters' error is estimated to perform a weighted least squares regression.

The basic idea exploited in all the aforementioned works is that forecasts can be reconciled solving a generalized least squares problem with error covariance matrix $\tilde{\Omega} \in \mathbb{R}^{n_r \times n_r}$:

$$\tilde{y}^T = S \underset{z}{\operatorname{argmin}} \|\hat{y}^T - S z^T\|_{\tilde{\Omega}^{-1}}^2 \quad (25)$$

which has an analytical solution. Imposing the first derivative to zero, we get:

$$\tilde{y}^T = S (S^T \tilde{\Omega}^\dagger S)^{-1} S^T \tilde{\Omega}^\dagger \hat{y}^T \quad (26)$$

where \dagger denotes the pseudo-inverse, since $\tilde{\Omega}$ is typically near-singular. Different hierarchical reconciliation methods basically differ in the choice and estimation of the error covariance matrix $\tilde{\Omega}$. We can see how (26) exploits only information of the originally forecasted signals, and from $\tilde{\Omega}$. The latter is usually estimated using forecast errors from a training set (or from all the available observations), and as such, can be considered invariant. We propose to use a MBT to estimate the reconciled signals starting from \hat{y} . This is easily obtained by setting the response to $r = S w$. Since S is fixed, following the same reasoning of the Fourier decomposition approach introduced in 4.1, equations (21) and (22) become:

$$w_l^* = -(\Lambda + n_l S^T S)^{-1} S^T G \quad (27)$$

$$\mathcal{L}_l^* = G^T S (\Lambda + n_l S^T S)^{-1} S^T G \quad (28)$$

The advantage of using a MBT over computing \tilde{y} is that we can use additional features to build the trees. We propose to fit the MBT on the residual between the observed signals and the bottom-up reconciliation, $y - \hat{y}_b S^T$, such that the final reconciled time series can be written as:

$$\tilde{y}_{mbt} = f(\{(\hat{y}_i, \epsilon_i, x_{t,i})_{i=1}^N\}) + \hat{y}_b S^T \quad (29)$$

where $\epsilon_i = \hat{y}_{t-1} - y_{t-1} \in \mathbb{R}^{N \times n_t}$ contains the forecast error at the timestep prior to the reconciliation and x_t contains categorical encoding of the weekday and the day-hour. Including ϵ_i in the tree features gives a possibility to the MBT to trust the forecast of the i_{th} predictor, based on its current performances.

4.3. Quantile loss and its relaxations

Quantile estimation in the context of boosting is usually achieved by minimizing the so-called quantile loss function, defined as:

$$l_q(\epsilon_{\tau_i}) = (\mathbb{1}_{\epsilon_{\tau_i} > 0} - \tau_i) \epsilon_{\tau_i} \quad (30)$$

where $\epsilon_{\tau_i} = y - \hat{q}_{\tau_i}$ is the distance between the observations and the predictions for the τ_i quantile. It can be shown that (30) is minimized when \hat{q}_{τ_i} is the τ_i quantile of F_Y , for any cdf F_Y . The quantile loss 30 is linear and asymmetric, with an undefined derivative at $\epsilon_{\tau_i} = 0$ and constant 0 Hessian. These characteristics make it hard to exploit the second-order approximation strategy. Indeed, relying only on the first-order approximation reduces the boosting strategy to fitting a classifier on the sign of ϵ_{τ_i} at each iteration k . Some popular boosted tree packages, like XGBoost, relax the loss function (30) considering a constant second derivative equal to 1. This has the practical effect

of fitting the k_{th} model f_k to the leaf-average binary response $\mathbb{I}_{\epsilon_{\tau_i} > 0}$. We propose a further relaxation of the problem, approximating the discontinuous gradient of the quantile loss function with a smooth function. The idea of smoothing the quantile loss for fitting boosted models was already introduced in (30), where the authors propose to use the cumulative density function of the Gaussian distribution ($\text{erf}(\epsilon_{\tau_i})$) as a smoothed version of the gradient of 30. The rationale behind smoothing l_q is that the MBT will have additional information on how far the observations are from the predicted quantile, which can help in building the tree. In this paper, we decided to use the (scaled and shifted) inverse logit function as a smoothed version of \tilde{l}_q derivative, due to its relation with logistic regression literature and the AdaBoost algorithm (see appendix Appendix B). This choice can be explained by the fact that the distance of the predicted τ_i quantile from the observation, i.e. ϵ_{τ_i} , is interpreted as the re-weighted log-odds of the condition $\epsilon_{\tau_i} > 0$. That is, if we describe y as the observation drawn from the random variable $Y(x)$, given the prediction $\hat{q}_{\tau_i}(x)$, we assume:

$$\epsilon_{\tau_i}(x) = y - \hat{q}_{\tau_i}(x) = \log \left(\frac{\tau_i F_{Y|x}}{(1 - \tau_i)(1 - F_{Y|x})} \right) \quad (31)$$

where $F_{Y|x}$ is the conditional cdf of Y , or the probability of $Y(x)$ being lower than the estimated quantile $\hat{q}_{\tau_i}(x)$. Inverting (31) we obtain:

$$F_{Y|x} = \frac{e^{\epsilon_{\tau_i}(x)-s}}{1 + e^{\epsilon_{\tau_i}(x)-s}} \quad (32)$$

where $s = \text{logit}(\tau_i)$. It can be easily verified that $F_{Y|x} = \tau_i$ when $\epsilon_{\tau_i} = 0$. In other words, we are implicitly assuming that the estimated quantile \hat{q}_{τ_i} is the correct one, under the hypothesis of Y having a logistic pdf:

$$h_{i,i} = dF_{Y|x} = \frac{e^{\epsilon_{\tau_i}-s}}{(1 + e^{\epsilon_{\tau_i}-s})^2} \quad (33)$$

where $h_{i,i}$ is the i_{th} diagonal element of the Hessian of the loss function. We can now define the smoothed derivative of $l_q(\epsilon_{\tau_i})$ as:

$$-g_k = -\frac{\partial \tilde{l}_q(\epsilon_{\tau_i})}{\partial f_k(x)} = \frac{\partial \tilde{l}_q(\epsilon_{\tau_i})}{\partial \epsilon_{\tau_i}} = F_{Y|x} - 1 + \tau_i \quad (34)$$

and we can now see that its second derivative is equal to the probability density function (33). Since $-1 + \tau_i$ is a constant, and at each iteration we fit $f_k(x)$ on $-g_k$, we can interpret the boosting procedure under the smoothed loss function as an iterative fitting on the probability $p_{Y < \hat{q}_{\tau_i}|x}$. We can see how the hypothesis on the distribution of the residuals we made in (31), and especially the τ_i re-weighting, has the effect of shifting \tilde{l}_q such that its minimum is located in $\epsilon_{\tau_i} = 0$. The effect of changing s can be seen in Fig. 1. As shown in Fig. 1, $\tilde{l}_q(\epsilon_{\tau_i})$ and its derivatives are now smooth functions, thus we can apply the same second-order approximation for fitting the multivariate tree, presented in section 3.2.

Linear-quadratic quantile loss function.

Smoothing $l_q(\epsilon_{\tau_i})$ has two main drawbacks. First, we cannot guarantee anymore its minimizer being the τ_i quantile of $F_{Y|x}$, independently from its distribution. In fact, any minimizer of

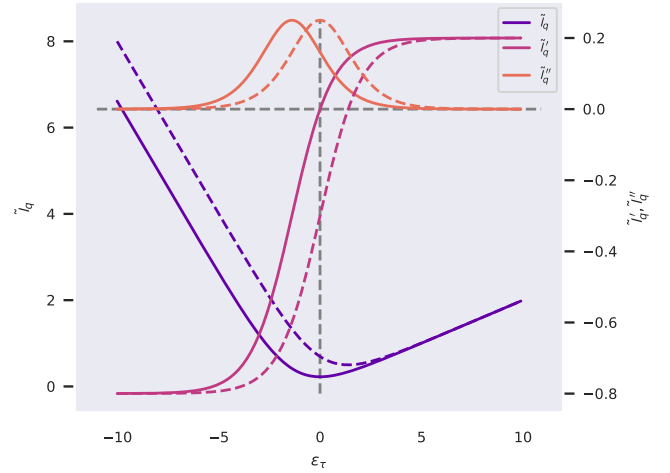


Figure 1: Continuous lines: smoothed quantile loss $\tilde{l}_q(\epsilon_{\tau_i})$ and its first and second derivatives for $\tau_i = 0.2$. Dashed lines: the same functions, for $s = 0$.

$\mathbb{E}(l_q(\epsilon_{\tau_i}))$ must zero its derivative, and this is true for any distribution $F_{Y|x}$ only if the derivative is independent from $F_{Y|x}$. The second drawback is that, as we try to mitigate the first effect by narrowing the pdf, the objective function becomes closer to the original quantile loss, turning the regression problem again in a classification one. Here we introduce a linear-quadratic quantile loss function which is consistent for any target pdf. We exploit the learning peculiarities of trees to approximate $F_{l,Y|x}$ in each leaf with the empirical one, $\hat{F}_{l,Y|x}$, and craft a smooth objective function whose minimizer is the empirical quantile of the $\hat{F}_{l,Y|x}$.

Theorem 1. Given a sample population $X_n = \{x_1, x_2, \dots, x_n\}$ and k being a constant, the following loss function:

$$l_{qs}(x, q, \tau_i) = \left((\tau_i - 1)x + \frac{kx^2}{2\bar{x}_l} \right) \mathbb{1}_{x < q} + \left(\tau_i x + \frac{kx^2}{2\bar{x}_r} \right) \mathbb{1}_{x \geq q} - 2x \quad (35)$$

where $\bar{x}_l = \sum_{i \in \mathbb{I}_l} x_i$, $\mathbb{I}_l = \{i : x_i < q\}$, $\bar{x}_r = \sum_{i \in \mathbb{I}_r} x_i$, $\mathbb{I}_r = \{i : x_i \geq q\}$, is minimized by the empirical quantile of X_n

The proof is reported in appendix Appendix A. The diagonal entries of the Hessian are then:

$$h_{i,i} = l_{qs}(x, q, \tau_i) = \left((\tau_i - 1) + \frac{kx}{\bar{x}_l} \right) \mathbb{1}_{x < q} + \left(\tau_i x + \frac{x}{\bar{x}_r} \right) \mathbb{1}_{x \geq q} - 2x \quad (36)$$

As recently introduced in the LightGBM implementation, we also consider the case of refitting the leaf responses w_l . After fitting the weak learner f_k using one of the approximated previously introduced losses, we replace w_l with the exact minimizers of (30), given the identified tree regions. That is, for each τ_i :

$$w_{l,i} = \hat{F}_{Y|x_l}^{-1}(\epsilon_{k,l,\tau_i}) \quad (37)$$

Section	\mathcal{L}	r	\tilde{G}	$\tilde{H} + \Lambda$
4.1	L2	w	ϵ	$n_l \mathbb{I}_{n_r} + \lambda D^T D$
4.1	L2	Pw	$P^T \epsilon$	$n_l \mathbb{I}_{n_r} + \Lambda$
4.2	L2	Sw	$S^T \epsilon$	$n_l S^T S + \Lambda$
4.4	L2	$x_l w$	ϵx^T	$x^T x + \Lambda$
4.3	$l_q(\epsilon_r)$	w	$(31) / (35)$	$(33) / (36)$

Table 1: List of combinations of loss and response functions, with their gradients and Hessians. First row: constant response with second derivative regularization. In rows 2, 3, 4 responses are linear functions of: nonlinear basis function, constant summation matrix, feature space. Last row: different quantile loss approximations with a constant response.

where ϵ_{k,l,τ_i} is the error at iteration k for the current leaf and quantile τ_i , while $\hat{F}_{Y|X_i}^{-1}$ is the inverse of the empirical conditional cdf of the current leaf.

4.4. Data driven control

Data-driven control (DDC) has been introduced in the last years as a way to overcome identification issues in model predictive control (MPC). The latter usually relies on the assumption that the controllable system obeys to linear time-invariant dynamics. However, for many systems of interest, a single linear system could not provide enough accuracy, while increasing the number of states or switching to a non-linear system can introduce identification issues and increase the computational time of the controller. The authors in [23, 24] introduce the idea of fitting a tree $f(x, \Theta)$, which responses are linearized dynamics of the controllable system. If the features used for growing the tree do not include control actions and system states, the linear dynamics identified in the leaves can be regarded as locally time-invariant and thus be used for control. Overcoming identifiability issues for control application is of great practical interest, and as such DDC gained popularity in the last year [25]. Here we propose to apply MBTs to increase the accuracy of the identified linear models, with respect to the one identifiable with a single tree. In this case, the weak learner $f(x, x_{lr}, \Theta)$ requires two sets of features: the one used to grow the tree and choose the best split, and the one used to fit the linear model in each leaf. Note that, due to the additive nature of boosting, the final model will still be a linear system in the tree's inputs. In this case, the second-order approximation is not helpful to reduce the calculation effort, because it corresponds to the exact solution of a linear system. We have, in fact:

$$w_l^* = -(\Lambda + x_{lr,l}^T x_{lr,l})^{-1} x_{lr,l}^T g_l \quad (38)$$

where $x_{lr,l} \in \mathbb{R}^{n_l \times n_f}$ is the feature matrix in the current leaf, and $g_l \in \mathbb{R}^{n_l \times n_l}$ is the gradient matrix in the current leaf.

4.5. Consistency

The additive nature of boosting guarantees consistency in the properties encoded in the weak learners, if they are in-

variant under summation. The two smoothing approaches presented in section 4.1 show different levels of consistency under boosting. For the Hodrick-Perscott filter, at each iteration, a curve with penalized second derivative is added in each leaf, such that the final curve is still smooth. However, if we compute the quadratic loss for the final response, $(\sum_{k=1}^{n_r} w_{l,k})^T D^T D (\sum_{k=1}^{n_r} w_{l,k})$ could be higher than the same loss from a single weak learner. This means that the final level of smoothness could depend on the number of fitting rounds n_r . For the Fourier expansion case, the final response will be a summation over Fourier coefficients in the chosen wave numbers $k \in \mathcal{K}$, which means the final signal will be a superposition of columns of P . This means that the Fourier decomposition property of identifying a signal composed only by harmonics with \mathcal{K} wave numbers is fully retained. The single fitted responses in section 4.2 respects the hierarchical relationship encoded in S , that is $r_k = S w_{l,k}$. Since S is constant through leaves and boosting rounds, also the final prediction retain this property, since $r = \sum_{k=1}^{n_r} S w_{l,k} = S \sum_{k=1}^{n_r} w_{l,k}$.

Quantile losses of section 4.3 do not generate strictly consistent responses. This is because the quantiles corrections identified at each iteration k are not jointly constrained. However, we will see in section 5.4 that in the case of the refitting strategy, consistency is respected in practice, presenting very few quantile crossing instances.

Finally, the prediction of MBT with linear responses of the feature space, like the one in section 4.4, is consistently linear in x , being a superposition of linear functions.

4.6. Numerical Methods

Table 1 summarizes the forms of the loss gradients and Hessian for the different combinations of losses and responses introduced in the previous section. In particular, the last column contains the expression that needs to be inverted when computing the optimal response w_l^* and approximated loss function. Inverting $\tilde{H} + \Lambda$ requires most of the computational time of the algorithm. Thus it is important to try to simplify or speed up this computation. In [7], the authors present an upper bound for the optimal response and loss in the case of a constant response and when the matrix $\tilde{H} + \Lambda$ is diagonally dominant. Here we show how to accelerate the exact computation of $(\tilde{H} + \Lambda)^{-1}$ for three of the cases in table 1. We can see how the first two cases require to invert a constant (through leaves and boosts) matrix, plus the identity matrix multiplied by the number of elements in the current leaf, n_l . This inversion can be reduced to a matrix multiplication thanks to the following theorem:

Theorem 2. *Given a symmetric invertible matrix $A \in \mathbb{R}^{k \times k}$, $(A + n\mathbb{I}_k)^{-1}$ can be computed as:*

$$(A + n\mathbb{I}_k)^{-1} = QLQ^{-1} \quad (39)$$

where $L \in \mathbb{R}^{k,k}$ is diagonal with $L_{i,i} = 1/(\lambda_i + n)$, λ_i is the i_{th} eigenvalue of A and Q is the matrix whose column are the eigenvectors of A .

The proof is reported in the appendix Appendix C. Since in our case A is constant, its eigenvalue, Q and its inverse can



Figure 2: Example of CV for 3 folds. Rows and columns indicate different folds and different times, respectively. Blue: training sets. Violet: test sets.

be computed only once for the entire fitting process. The only variable part is n , which in our case corresponds to the number of observations in the current leaf. This only affects the diagonal entries of L , while all the other quantities in the right-hand side of (39) remain unchanged. For the third case of table 1, we have to invert $n_l S^T S + \Lambda$. Once again, the only non-constant term is n_l . If the quadratic punishment term Λ is a multiple of the identity matrix (as is typically assumed), this can be written as $n_l S^T S + n \mathbb{I}$, and we can use the following corollary of the previous theorem:

Corollary 1. *Given a symmetric invertible matrix $A \in \mathbb{R}^{k \times k}$, $(mA + n\mathbb{I}_k)^{-1}$ can be computed as:*

$$(mA + n\mathbb{I}_k)^{-1} = QLQ^{-1}/m \quad (40)$$

where $L \in \mathbb{R}^{k,k}$ is diagonal with $L_{i,i} = 1/(\lambda_i + n/m)$, and λ_i and Q as defined in 2.

the latter corollary follows from theorem 2 proof, noting that $mA + n\mathbb{I}_k = m(A + n\mathbb{I}_k/m)$.

5. Numerical results

In this section, we present numerical results of the responses and loss functions introduced in section 4. For all the datasets, we obtained the results using k-fold cross-validation (CV). Since all the applications deal with temporal data, we adopted sliding-window cross-validation. An example of training and testing splits under this cross-validation is shown in Fig. 2, in the case of 3 folds.

5.1. Forecasting via Fourier decomposition

We applied the Fourier-based MBT introduced in 4.1 to a publicly available dataset of power demand time series [26]. The dataset consists of about 1 year of electrical load measurements of secondary substations and cabinets located in a low voltage distribution grid. The signals have a sampling frequency of 10 minutes. In total, 31 time series are provided, showing hierarchical relationships, that is, 7 time series are the algebraic summation of specific subgroups. Called P_i the power measurement of the i_{th} time series, we aim at forecasting the day-ahead signal (144 steps), given only historical values and time-related covariates:

$$\hat{P}_{i,k} = f((P_{i,t-j}, x_t)_{j=1}^N) \quad (41)$$

where x_t contains categorical encodings of the weekday and the day-hour, and $k \in [1, 144]$ and $j \in [1, 1008]$, corresponding to 24 hours ahead and a history of 1 week, with a sampling time of 10 minutes. We adopted the same procedure explained in detail in [27] for the construction of the feature matrix $((P_{i,t-j}, x_t))$. We compared the MBT with two baselines

using LightGBM and two different multi step-ahead strategies [28]. The first one mimics a multiple-input multiple-output approach (MIMO). This is obtained, similarly to what is done in [29] with support vector machines, by adding an auxiliary feature $x_{c,i}$ to the dataset, which represents a categorical encoding of the step ahead to which y_i corresponds. The second one adopts a multiple-input single-output (MISO) approach: 144 different models are trained, each of them predicting a given step ahead. This strategy has the advantage of increasing the final forecaster flexibility, at the price of disregarding time correlations in the predictions.

An example of 24 hours ahead Fourier forecasting using an increasing number of harmonics is shown in Fig. 3. The top panel shows the aggregated time series, while the second panel shows one of the bottom (more variable) time series. It can be seen how increasing the number of harmonics (from dark to light colours) increases the flexibility of the forecaster while keeping potential useful time correlations. However, in this case, the targets present a degree of correlation which depends on the hour of the day. In the top panel of Fig. 3 it can be seen how the target is strongly correlated in the early morning and during evening hours, while correlation is less obvious in during the day. This pattern is recurrent in all the days of the dataset. To see the effect of the number of harmonics on the accuracy of the MBT, we retrieve the forecasts for all the 31 time series using a 3 fold CV, for an increasing number of wavenumbers. This investigation is reported in Fig. 4, where the CV fold-mediated and normalized RMSE and MAPE are reported. The first column uses the values of the RMSE and MAPE from the MIMO strategy benchmark for the normalization of the results, while the second one normalizes the MBT key performance indicators (KPIs) with the one obtained with the MISO strategy. Dots highlights the best normalized performance for the various time series, while colours represent the MAPE obtained with MIMO (first column) and MISO (second column) strategies. We can see how the MBT is strictly better than the MIMO strategy in terms of RMSE, for almost all the number of harmonics, while achieving better results in terms of MAPE for 2 over 31 cases. Despite the lack of inter-temporal information, the MISO strategy performs better than the other two on average. The MBT provides higher accuracy for 10 time series in terms of RMSE and for 7 in terms of MAPE. However, no evident correlation with respect to the MISO strategy MAPE (line colour) is observed.

In all the cases, we can observe an initial improvement of performances with respect to increasing wavenumber. Results show that the minimum of the KPIs lies in what looks like a plateau for all the considered cases, as the wavenumber increases. This means that while considering more harmonics than the one highlighted by the dots, the accuracy does not increase or decrease significantly. This suggests that including a priori information on the smoothness (and time correlation structure) of the curve doesn't seem to be particularly helpful for this dataset.

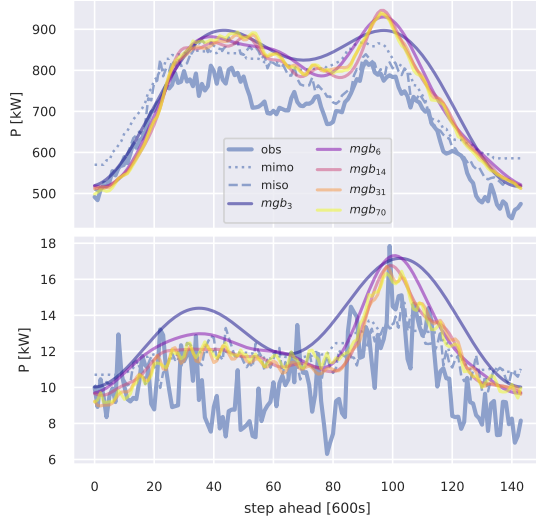


Figure 3: Example of forecasting via Fourier decomposition on the aggregated time series (top) and on time series belonging to the lower aggregation level (bottom). Thick blue line represents the ground truth, while the dotted and dashed lines represents the mimo and miso benchmarks. The other lines are forecasts obtained with MBT, the color indicating an increasing number of considered frequencies, from darker to lighter.

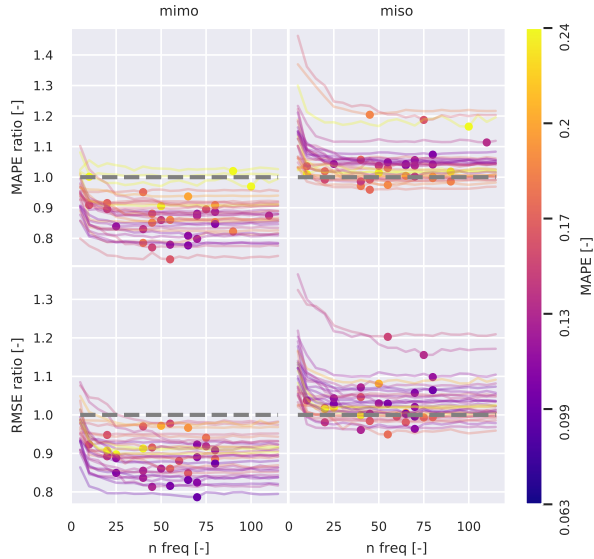


Figure 4: RMSE and MAPE, mediated over CV folds and step ahead, for a different number of harmonics fitted by the forecaster based on Fourier decomposition. In the first column, the KPIs are normalized with the KPIs of the MIMO forecaster, while in the second one they are normalized with the KPIs of miso strategy. Colours in the first and second column refer to the MAPE of the MIMO and MISO strategy, respectively.

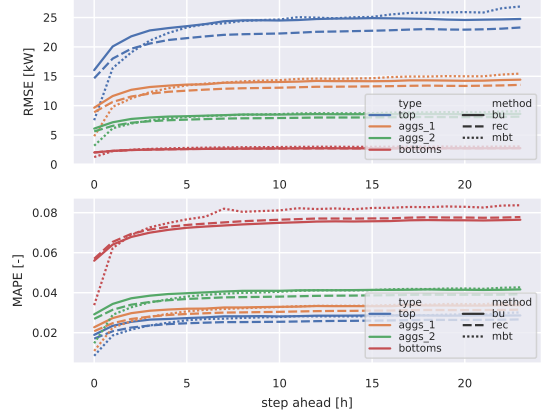


Figure 5: RMSE as a function of the step ahead, grouped by hierarchical levels, mediated over the CV folds, for different reconciliation techniques. Blue, orange, green and red lines refer to the overall aggregated profile, the first and second level of aggregates, and the bottom time series, respectively. Continuous lines: bottom-up reconciliation. Dashed lines: reconciled forecasts using the shrink strategy and glasso covariance estimation. Dotted lines: MGB with history of reconciliation errors.

5.2. Hierarchical forecasting

Using the same dataset of the previous section, we obtained the baseline 24 hours ahead forecasts for all the 31 time series, using 3 fold CV. In this dataset we have 3 aggregation levels, so that the summation matrix S can be written as:

$$S = \begin{bmatrix} \mathbb{1}_{n_b} \\ I_2 \otimes \mathbb{1}_{n_b/2} \\ I_4 \otimes \mathbb{1}_{n_b/4} \\ I_{n_b} \end{bmatrix} \quad (42)$$

where $\mathbb{1}_{n_b}$ is the unit row vector with the size equal to the number of bottom-level time series, in this case, $n_b = 24$ and \otimes is the Kronecker product. The forecasts are then reconciled using the minT strategy [22], coupled with the graphical Lasso approach [30] for the error covariance estimation and a bottom-up strategy. The latter consist in retrieving consistent forecast summing up bottom level forecasts. Formally, we obtain the set of reconciled forecasts as $\tilde{y} = S \hat{y}_b$. We then compare the results with a MBT using information about the forecast error of the previous timestep, as described in section 4.2. The results as a function of the step ahead, and divided by aggregation groups, are presented in Fig. 5. We can see how the additional information that MBT can exploit significantly decrease the forecast error for the first hours ahead. On the other hand, the advantage over standard reconciliation approaches vanishes with the increase of the step-ahead. Since the MBT requires substantially more computational time, an effective strategy would be to fit this model only for the initial steps ahead and then switch to the standard reconciliation strategy.

5.3. Boosted voltage sensitivity coefficients

While DDC has been mainly applied to the control of heating systems, here we propose an application for the control in the electrical distribution grid. When performing optimal power flow, a distribution system operator (DSO) must take into account the nonlinear power flow equation, which includes the nonlinear relation:

$$S = V \odot I^* \quad (43)$$

where S , V and I are the vectors of complex powers, voltages and currents in the buses of the network, $*$ denotes the complex conjugate and \odot the Hadamard product. Different relaxations of power flow equation exist [31]. Usually, either the knowledge of phasors' angles (e.g. DC approximation) or the knowledge of the lines' parameters and topology (e.g. the DistFlow model) are required inputs to this approximation. However, this information is not always available. For example, the network topology of the low-voltage grid, where most residential users are located, is usually unknown or difficult to access. In the absence of network topology, one could opt for an approximate formulation of the power flow, whose parameters can be estimated using smart meter data. One of these formulations consists of the first-order linearization of the power flow equations. The linear coefficients of this formulation are known as the voltage sensitivity coefficients (VSCs):

$$k_{i,j}^p = \frac{\partial |V_j|}{\partial P_k} \quad k_{i,j}^q = \frac{\partial |V_j|}{\partial Q_k} \quad (44)$$

where P and Q are the active and reactive power, respectively, and $k_{i,j}^p, k_{i,j}^q$ are the sensitivity coefficients between node i and node j . The analytical expression of voltage sensitivity coefficients, and an efficient method to compute them based on the state of the grid and admittance matrix, is provided in [32]. In [33], it has been shown that the voltage sensitivity coefficients can be estimated by least-squares regression of the time derivatives of voltage magnitudes, P and Q . We follow their approach to find sets of VSCs, conditional to the state of the grid. However, knowing the latter would require to know all the voltages of the buses' grid. As discussed in section 4.4, we aim at building the MBT without using the state of the system, we use the power measurements at the point of common coupling (PCC) with the medium voltage grid as a proxy for the state of the grid.

In order to compare the approach in [33] with the MBT one, we simulated 3 months of data for a low voltage grid located in Switzerland. Fig. 6 show the topology of the grid and the QP buses locations. This information, along with parameters for the grid's cables, were retrieved from the local DSO. Power profiles of uncontrollable loads were generated with the LoadProfileGenerator [34]; power profiles of photovoltaic roof-mounted power plants were obtained through the PVlib python library [35], while the electrical loads due to heat pumps was retrieved simulating domestic heating systems and buildings thermal dynamics, modelling them starting from building's metadata. The grid was then simulated with OpenDSS [36], and the 3 phases voltages, power and currents retrieved for all the QP nodes of the grid, with a 1 minute sampling time.

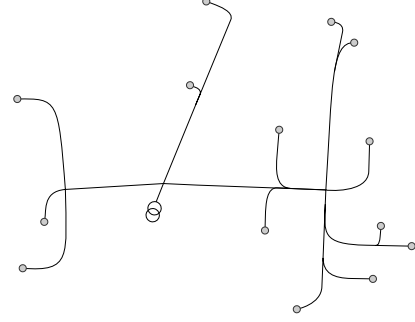


Figure 6: Schematics of the simulated low voltage grid for the VSC computation. Grey circles indicates single households, while the double circle indicate the power transformer.

The results were then obtained by applying a 10 fold CV. As an additional comparison, we considered Ridge regression for the VSCs. Since x_{lr} and y both have a high number of dimensions, quadratic coefficient punishment could help in finding a better solution. The punishment coefficient for the Ridge regression was found using an inner CV for each fold. The dataset for the linear regression was $\mathcal{D} = \{(x_{lr,i}, y_i)_{i=1}^N\}$ is the same for all the three models, where $x_{lr} \in \mathbb{R}^{N \times 6n}$ contains the discrete-time derivatives of P and Q values for the 3 phases of all the buses, while $y \in \mathbb{R}^{N \times 3n}$ contains the time derivatives of the voltages. The MBT was built using $x \in \mathbb{R}^{N \times 3}$, which contains P_{PCC} , which is the power measured at the PCC (the double circle in Fig. 6), the hour of the day and the weekday. In this case, the tree growth is not independent from the control action, since the power at PCC includes the power of controlled appliances in the grid. Under these conditions, the MBT can still be applied to build an oracle for checking voltage violations, using a "proxy-Lagrangian" formulation of the optimization problem [37]. However, this results in a more complex formulation, being the constraints non-convex. We compare this solution to one in which the MBT is only fitted using meteorological variables, i.e. the ambient temperature T_a and the solar irradiance G_{irr} , the hour of the day and the weekday. In this case the identified leaves are independent from system state and control actions, and as such the MBT can be employed in standard convex optimization.

Fig. 7 shows results in terms of mean RMSE over folds and grids' nodes, and of normalized RMSE. The normalization of the latter is done with the mean RMSE obtained with a constant prediction of the voltage. This is a meaningful normalization because in Europe voltage signals in low voltage networks have a nominal value of 230V, and usually they do not deviate more than the 10%. Ridge regularization slightly increase the accuracy, while the MBT does it significantly. As expected, the MBT using power at PCC is more accurate with respect to its counterpart using only disturbances for the growth of the trees. This means that the power at the PCC is a better proxy for the state of the electrical grid than the meteorological variables. However, since these models are meant to be used in control applications, the models must be accurate for the whole decision horizon (typically 24 hours ahead for demand-side management applications). Since the first two models are constant, they do

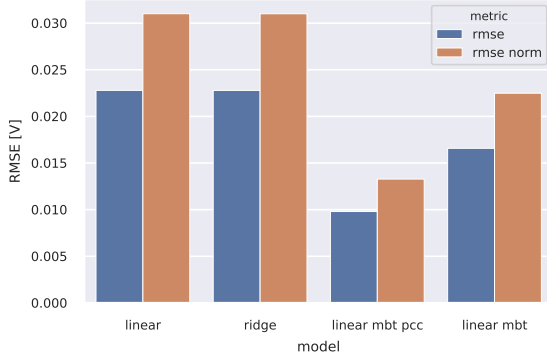


Figure 7: RMSE for different regressors, mediated over the CV folds and nodes. The red columns show the RMSE normalized with the predictions using the sample mean values.

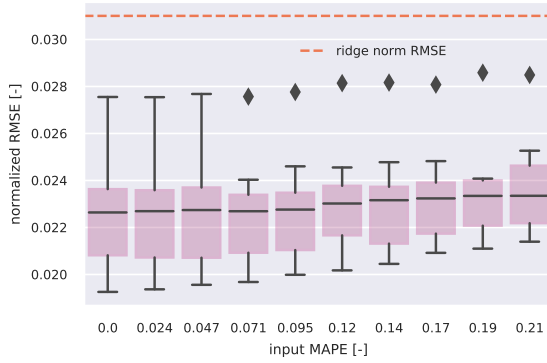


Figure 8: Boxplots for the 10 fold CV of the normalized RMSE of the MBT predictor for increasing levels of noise in the tree inputs, in terms of MAPE.

not need any further investigation. On the other hand, the final MBT model depends on the features used to build the tree, x . In the following we restrict the analysis to the MBT fitted on the meteorological variables; the one fitted on P at PCC shows a very similar behavior. Indeed, we only need to investigate the accuracy degradation with respect to the forecasted T_a and G_{irr} , since the other two variables in x are deterministic. We thus applied increasing levels of multiplicative noise from a (3σ) truncated Gaussian distribution to T_a and G_{irr} , to mimic accuracy degradation in its forecasts, and retrieved the MBT normalized RMSE on the CV folds. The results are shown in Fig. 8 in terms of increasing MAPE on the forecasted T_a and G_{irr} signals, as box plots containing the 10 CV folds measurements. We can conclude that the degradation of the MBT is negligible up to a MAPE of 21%, which corresponds to very bad forecasts for this kind of applications.

5.4. Quantile prediction

We tested the different quantile loss relaxations and fitting strategies presented in section 4.3 on the aggregated power profile of the hourly-resampled dataset [26]. In particular, we seek to retrieve the quantile predictions tensor $\hat{q}_{\tau_i} \in \mathbb{R}^{N \times n_t \times n_q}$ where $\tau_i \in \mathcal{T}$, \mathcal{T} is a set of $n_q = 11$ equispaced quantiles and $n_t = 24$. For all the methods, we kept the same features and target matrix x and y as specified in section 5.1. The benchmark to which we compare the MBT-based solutions are 24 sets of n_q LightGBMs, that is, we fitted a different LightGBM for each combination of step-ahead and quantile. Other three models are then compared: the MBT using the smoothed version of quantile loss \tilde{l}_q , defined by its gradient (34) and Hessian (33); the same model with quantile refitting, as explained in section 4.3; the model using the linear-quadratic quantile loss defined by its gradient (35) and Hessian (36), with quantile refitting.

Quality of quantile forecasts is harder to assess compared to point forecasts since different desirable properties of the forecasted prediction interval must be evaluated. For this comparison we relied on 4 KPIs. The first one is the time average of the quantile loss (30), $\bar{l}_q = \sum_{t=1}^T l_q(\epsilon_{\tau_i,t})$. The second one is the quantile score $Qs(\hat{q}_{\tau_i}, y)$, which is a proper scoring rule [38, 39, 40], and it's defined as the expected quantile loss (30):

$$Qs = \int_0^1 \bar{l}_q(\epsilon_{\tau_i}) d\tau_i \approx \sum_{\tau_i \in \mathcal{T}} \bar{l}_q(\epsilon_{\tau_i}) d\tau_i \quad (45)$$

where \hat{q}_{τ_i} is the predicted τ_i -quantile, while y is the observed ground truth. This score is strictly connected with the continuous rank probability score [38], both being total variation measurements between the forecasted pdf and a Heaviside distribution centred on the observation y . For these scores, lower values indicate better performances. The third KPI is based on the reliability [41], which is the average number of times the observed signal was actually below the predicted τ quantile.

$$r_{\tau_i} = \frac{1}{N} \sum_{j=1}^N \mathbb{1}_{\{y_j < \hat{q}_{\tau_i,j}\}} \quad (46)$$

When plotted against \mathcal{T} , the perfect reliability aligns with the bisector of the first quadrant. Because all the models provided highly reliable quantiles, to ease the comparison of the performance, we defined the following KPI:

$$Rs = |r_{\tau_i}(F_b) - \tau| - |r_{\tau_i}(F_m) - \tau| \quad (47)$$

that is, the difference of absolute deviation from the perfect reliability, between a benchmark forecasting model F_b and the considered one, F_m . The last KPI is the mean crossing of the quantiles. We define it as:

$$\bar{\chi} = \frac{1}{n_q} \sum_{i=1}^{n_q} \frac{1}{N} \sum_{j=1}^N \mathbb{1}_{\{\hat{q}_{\tau_i} > \hat{q}_{\tau_{i+1}}\}} \quad (48)$$

that is, the average over quantiles of the mean number of times \hat{q}_{τ_i} violates the monotonicity of $\hat{F}(Y)$.

In Fig. 10 we compare the quantile loss $l_q(\epsilon_{\tau_i})$ as a function of τ_i and the step ahead. To ease the comparison, we plot the

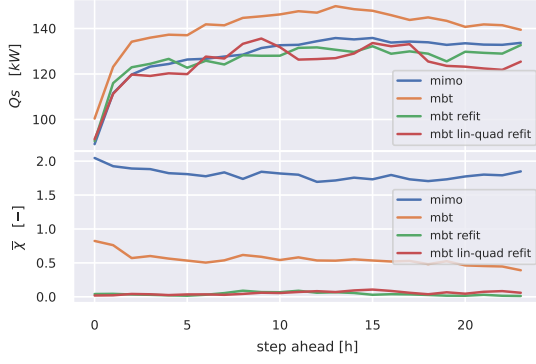


Figure 9: CRPS and mean quantile crossings, as a function of step-ahead, mediated over the CV folds. The refitted MGB with logistic and quadratic losses show similar performances with the MISO strategy while achieving a significantly lower number of crossings.

differences between the $l_q(\epsilon_{\tau_i})$ of the benchmark and the other models. The original quantile loss plots can be found in the appendix Appendix D. The first MBT model presents a sparser forecasted pdf compared with the benchmark, while the refitted models are consistently better at modelling the tails of the distribution. As shown in Fig. 11, however, the first MBT model shows significantly higher reliability with respect to the benchmark, especially in the tails of the distribution. This gain is somehow lower in the two refitted models, which, on the other hand, have narrower pdfs. The same conclusion on the sharpness of the estimated distributions can be drawn from the first panel of Fig. 9, which shows the quantile score Q_s as a function of step-ahead for the four different models. While the MBT with smoothed loss function estimate sparser pdfs, the model exploiting the refitting strategy shows a Q_s comparable with the benchmark, while the last model is strictly better for most of the steps ahead. The second panel shows \bar{x} for increasing steps ahead. It is evident how using different BTs for different quantiles leads the benchmark model to inconsistent results. The quantile crossing is considerably lower for the MBT based on the smoothed loss function while being negligible for the models using refitting.

6. Conclusions

In this paper, we have presented a multivariate boosted tree algorithm, fitted in parameter space, using the same second-order Taylor expansion used by LightGBM and XGboost. The algorithm allows to arbitrarily regularize the predictions, through the use of multivariate penalization and basis functions. We have shown how, for a relevant class of applications, the Hessian inversion required for fitting the underlying tree models can be reduced to a matrix multiplication, making the algorithm computationally appealing. Unlike its univariate counterpart, the MBT is particularly useful when properties like smoothness, consistency and functional relations are required.

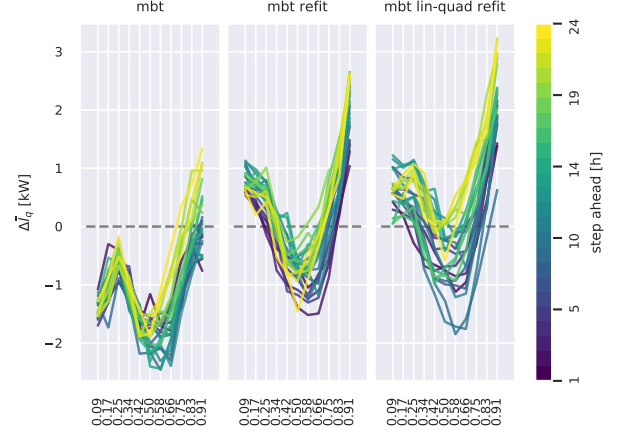


Figure 10: Differences between \bar{l}_q for different models, with respect to the benchmark case, as a function of τ_i and the step ahead (line colour, from blue to yellow). Lines above the grey dashed line denotes better performances. The refitted model shows more accurate predictions in the tails of the distribution compared to the benchmark.

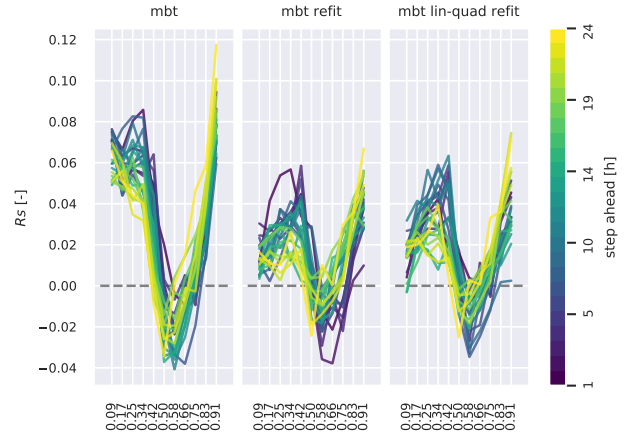


Figure 11: R_s for different models, with respect to the benchmark case, as a function of τ_i and the step ahead (line colour, from blue to yellow). All the models show more reliable quantiles in the tails of the distribution compared to the benchmark.

We have shown this through numerical examples on four different tasks, namely: time series forecasting, hierarchical reconciliation, data-driven control and quantile forecasting. While including a priori regularization on the smoothness of a forecasted time series doesn't seem to increase accuracy against univariate BTs with a MISO strategy, for the other presented applications, where some consistency is explicitly required, the algorithm showed clear advantages. We conclude by noting that the presented MBT algorithm only used histogram-based split search since we did not make use of very large datasets in our experiments. Computational time can be readily reduced through the adoption of numerical techniques tailored to tree fitting, such as gradient-based one-side sampling and exclusive feature bundling [8].

Appendix A. Proof of theorem 1

Proof. The loss function (35) is minimized in expectation, with respect to the empirical distribution of X_n , if the expectation of its derivative is zero by its minimizer:

$$q^* = \underset{q}{\operatorname{argmin}} \mathbb{E}_{X_n} l_{qs}(x, q, \tau_i) \quad (\text{A.1})$$

$$q^* \text{ s.t. } \frac{\partial \mathbb{E}_{X_n} l_{qs}(x, q^*, \tau_i)}{\partial q} = 0 \quad (\text{A.2})$$

Keeping the same nomenclature in theorem (1), we retrieve x^* by solving (A.2). We start by calculating $\frac{\partial \mathbb{E}_{X_n} l_{qs}}{\partial q}$:

$$\begin{aligned} \frac{\partial \mathbb{E}_{X_n} l_{qs}}{\partial q} &= 2k - \sum_{i \in \mathbb{I}_l} \tau_i - 1 + \frac{kx_i}{\bar{x}_l} - \sum_{i \in \mathbb{I}_r} \tau_i + \frac{kx_i}{\bar{x}_l} \\ &= rk(q)(\tau_i - 1) - (1 - rk(q))\tau_i \\ &= rk(q) - \tau_i \end{aligned}$$

where $rk(q)$ is the rank of q with respect to the samples in X_i . Thus, equating the last expression to 0, we find that $rk(q^*) = \tau_i$, that is, q^* is the empirical τ_i quantile of X_n . \square

Appendix B. Connections with AdaBoost

At each iteration, AdaBoost employs an exponential loss function in order to solve a binary classification problem. It can be shown that the minimizer $f_k^*(x)$ of this loss minimizes also the logit loss associated to the classification probabilities [42]:

$$f_k^*(x) = \underset{f_k(x)}{\operatorname{argmin}} l_A(y, f_k(x)) = \log \left(\frac{P_{\{y=1|x\}}}{P_{\{y=-1|x\}}} \right) \quad (\text{B.1})$$

and therefore, inverting this relation, the conditional probability $p(y = 1|x)$ can be written as:

$$p(y = 1|x) = \frac{e^{f_k^*(x)}}{e^{-f_k^*(x)} + e^{f_k^*(x)}} = \frac{e^{2f_k^*(x)}}{1 + e^{2f_k^*(x)}} \quad (\text{B.2})$$

which means that AdaBoost algorithm can be explained in terms of an additive logistic regression model.

Appendix C. Proof of theorem 2

Proof. Considering the eigenequation of matrix A :

$$Ax = \lambda x \quad (\text{C.1})$$

and adding a multiple of the identity matrix:

$$(A + n\mathbb{I})x = (\lambda + n)x \quad (\text{C.2})$$

calling $A + n\mathbb{I} = \tilde{A}$, this means that $\lambda_{\tilde{A},i} = \lambda_{A,i} + n$, where $\lambda_{A,i}$ denotes the i_{th} eigenvalue of A . Since adding a multiple of \mathbb{I} to A just influences the magnitude of the vector to which the final matrix is applied, the eigenvectors of A and $A + n\mathbb{I}$ are the same. Thus, since A is symmetric and invertible, and its inverse can be obtained as:

$$A^{-1} = Q^T L Q \quad (\text{C.3})$$

\tilde{A} can be obtained as

$$\tilde{A}^{-1} = Q^T \tilde{L} Q \quad (\text{C.4})$$

where $L \in \mathbb{R}^{k,k}$ is diagonal with $L_{i,i} = 1/\lambda_{A,i}$ and $\tilde{L} \in \mathbb{R}^{k,k}$ is diagonal with $\tilde{L}_{i,i} = 1/(\lambda_{A,i} + n)$. \square

Appendix D. Additional figures

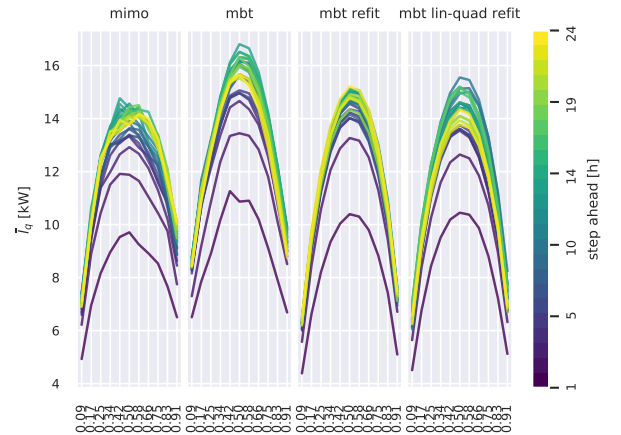


Figure D.12: \tilde{l}_q for different models, as a function of τ_i and the step ahead (line color, from blue to yellow).



Figure D.13: Reliability plots for different models, as a function of τ_i and the step ahead (line color, from blue to yellow).

References

- [1] B. N. Oreshkin, D. Carпов, N. Chapados, Y. Bengio, N-BEATS: Neural basis expansion analysis for interpretable time series forecasting (2019) 1–31 arXiv:1905.10437. URL <http://arxiv.org/abs/1905.10437>
- [2] S. Belharbi, R. Héroult, C. Chatelain, S. Adam, Deep neural networks regularization for structured output prediction, *Neurocomputing* 281 (2018) 169–177. arXiv:1504.07550, doi:10.1016/j.neucom.2017.12.002. URL <https://doi.org/10.1016/j.neucom.2017.12.002>
- [3] M. M. Bronstein, J. Bruna, Y. Lecun, A. Szlam, P. Vandergheynst, Geometric Deep Learning: Going beyond Euclidean data, *IEEE Signal Processing Magazine* 34 (4) (2017) 18–42. arXiv:1611.08097, doi:10.1109/MSP.2017.2693418.
- [4] LightGBM - Release 2.3.2, Tech. rep. (2020). URL <https://readthedocs.org/projects/lightgbm/downloads/pdf/latest/>
- [5] A. Pande, L. Li, J. Rajeswaran, J. Ehrlinger, U. B. Kogalur, E. H. Blackstone, H. Ishwaran, Boosted multivariate trees for longitudinal data, *Machine Learning* 106 (2) (2017) 277–305. doi:10.1007/s10994-016-5597-1.
- [6] W. Li, W. Wang, W. Huo, RegBoost : a gradient boosted multivariate regression algorithm, *International Journal of Crowd Science* (61672384) (2019). doi:10.1108/IJCS-10-2019-0029.
- [7] Z. Zhang, C. Jung, GBDT-MO: Gradient Boosted Decision Trees for Multiple Outputs (2019) 1–13 arXiv:1909.04373. URL <http://arxiv.org/abs/1909.04373>
- [8] G. Ke, Q. Meng, T. Finley, T. Wang, W. Ma, Q. Ye, T.-Y. Liu, LightGBM: A Highly Efficient Gradient Boosting Decision Tree, *Nips '17* (Nips) (2017) 9. URL <https://github.com/Microsoft/LightGBM>.
- [9] Y. Freund, R. E. Schapire, A Decision-Theoretic Generalization of On-Line Learning and an Application to Boosting, *Journal of Computer and System Sciences* (1997). doi:10.1006/jcss.1997.1504.
- [10] P. Bühlmann, T. Hothorn, Boosting algorithms: Regularization, prediction and model fitting, *Statistical Science* (2007). doi:10.1214/07-STS242.
- [11] L. Breiman, Arcing classifiers, *Annals of Statistics* (1998). doi:10.1214/aos/1024691079.
- [12] J. H. Friedman, Greedy function approximation: A gradient boosting machine, *Annals of Statistics* (2001). doi:10.2307/2699986.
- [13] T. Duan, A. Avati, D. Y. Ding, S. Basu, A. Y. Ng, A. Schuler, NGBoost: Natural Gradient Boosting for Probabilistic Prediction (2019). arXiv:1910.03225. URL <http://arxiv.org/abs/1910.03225>
- [14] T. Chen, C. Guestrin, XGBoost: A Scalable Tree Boosting System, *Proceedings of the 22Nd ACM SIGKDD International Conference on Knowledge Discovery and Data Mining* (2016) 785–794 arXiv:1603.02754, doi:10.1145/2939672.2939785.
- [15] M. Mehta, R. Agrawal, J. Rissanen, SLIQ: A fast scalable classifier for data mining, in: *Lecture Notes in Computer Science (including subseries Lecture Notes in Artificial Intelligence and Lecture Notes in Bioinformatics)*, 1996. doi:10.1007/bfb0014141.
- [16] S.-J. Kim, K. Koh, S. Boyd, D. Gorinevsky, Trend Filtering., *SIAM Review* 51 (2) (2009) 339–360. doi:10.1137/070690274. URL [10.1137/070690274%5Cnhttp://ezaccess.libraries.psu.edu/login?url=http://search.ebscohost.com/login.aspx?direct=true&db=a9h&AN=42745372&site=ehost-live&scope=site](http://ezaccess.libraries.psu.edu/login?url=http://search.ebscohost.com/login.aspx?direct=true&db=a9h&AN=42745372&site=ehost-live&scope=site)
- [17] R. M. de Jong, N. Sakarya, The econometrics of the Hodrick-Prescott filter, *Review of Economics and Statistics* (2016). doi:10.1162/REST_a_00523.
- [18] J. O. Ramsay, G. Hooker, S. Graves, Smoothing: Computing Curves from Noisy Data, Springer New York, New York, NY, 2009, pp. 59–82. doi:10.1007/978-0-387-98185-7_5. URL https://doi.org/10.1007/978-0-387-98185-7_5
- [19] A. J. Izenman, Reduced-rank regression for the multivariate linear model, *Journal of Multivariate Analysis* 5 (2) (1975) 248–264. doi:10.1016/0047-259X(75)90042-1.
- [20] R. J. Hyndman, R. A. Ahmed, G. Athanasopoulos, H. L. Shang, Optimal combination forecasts for hierarchical time series, *Computational Statistics and Data Analysis* (2011). doi:10.1016/j.csda.2011.03.006.
- [21] S. L. Wickramasuriya, G. Athanasopoulos, Optimal forecast reconciliation for hierarchical and grouped time series through trace minimization, *Journal of the American Statistical Association* (2017).
- [22] S. L. Wickramasuriya, G. Athanasopoulos, R. J. Hyndman, Forecasting hierarchical and grouped time series through trace minimization, *Journal of the American Statistical Association* (November) (2018). doi:10.1080/01621459.2018.1448825.
- [23] A. Jain, M. Behl, R. Mangharam, Data Predictive Control for building energy management, *Proceedings of the American Control Conference* (May) (2017) 44–49. doi:10.23919/ACC.2017.7962928.
- [24] F. Smarra, A. Jain, T. de Rubéis, D. Ambrosini, A. D’Innocenzo, R. Mangharam, Data-driven model predictive control using random forests for building energy optimization and climate control, *Applied Energy* 226 (2018) 1252–1272. doi:10.1016/j.apenergy.2018.02.126.
- [25] Special Issue “Energy Efficiency and Data-Driven Control”, *Energies* (ISSN 1996-1073) (2019).
- [26] <https://zenodo.org/record/3463137#XY3GqvexWV4>.
- [27] L. Nespoli, V. Medici, K. Lopatichki, F. Sossan, Hierarchical Demand Forecasting Benchmark for the Distribution Grid, accepted, in: *PSCC 2020*, 2019. arXiv:1910.03976. URL <http://arxiv.org/abs/1910.03976>
- [28] S. Ben Taieb, G. Bontempi, A. F. Atiya, A. Sorjamaa, A review and comparison of strategies for multi-step ahead time series forecasting based on the NN5 forecasting competition, *Expert Systems with Applications* 39 (8) (2012) 7067–7083. arXiv:1108.3259, doi:10.1016/j.eswa.2012.01.039. URL <http://dx.doi.org/10.1016/j.eswa.2012.01.039>
- [29] A. K. Sampathirao, J. M. Grosso, P. Sopasakis, C. Ocampo-Martinez, A. Bemporad, V. Puig, Water demand forecasting for the optimal operation of large-scale Drinking Water Networks: The barcelona case study, in: *IFAC Proceedings Volumes (IFAC-PapersOnline)*, 2014. doi:10.3182/20140824-6-za-1003.01343.
- [30] J. Friedman, T. Hastie, R. Tibshirani, Sparse inverse covariance estimation with the graphical lasso, *Biostatistics* (2008). doi:10.1093/biostatistics/kxm045.
- [31] D. K. Molzahn, F. Dörfler, H. Sandberg, S. H. Low, S. Chakrabarti, R. Baldick, J. Lavaei, A Survey of Distributed Optimization and Control Algorithms for Electric Power Systems, *IEEE Transactions on Smart Grid* 3053 (c) (2017) 1. doi:10.1109/TSG.2017.2720471.
- [32] K. Christakou, J. Y. Leboudec, M. Paolone, D. C. Tomozei, Efficient computation of sensitivity coefficients of node voltages and line currents in unbalanced radial electrical distribution networks, *IEEE Transactions on Smart Grid* 4 (2) (2013) 741–750. arXiv:arXiv:1203.6798v2, doi:10.1109/TSG.2012.2221751.

- [33] C. Mugnier, K. Christakou, J. Jatón, M. De Vivo, M. Carpita, M. Paolone, Model-less/measurement-based computation of voltage sensitivities in unbalanced electrical distribution networks, 19th Power Systems Computation Conference, PSCC 2016 (2016). doi:10.1109/PSCC.2016.7540852.
- [34] N. Pflugrad, J. Teuscher, B. Platzer, W. Schufft, Analysing low-voltage grids using a behaviour based load profile generator, Renewable Energy and Power Quality Journal (2013). doi:10.24084/repqj11.308.
- [35] R. W. Andrews, J. S. Stein, C. Hansen, D. Riley, C. Consulting, S. N. Laboratories, Introduction to the Open Source PV LIB for Python Photovoltaic System Modelling Package (2012).
- [36] R. C. Dugan, The Open Distribution System Simulator (OpenDSS), Tech. rep. (2012).
- [37] A. Cotter, H. Jiang, K. Sridharan, Two-Player Games for Efficient Non-Convex Constrained Optimization 98 (1) (2019) 1–33. arXiv:1804.06500.
URL <http://arxiv.org/abs/1804.06500>
- [38] T. Gneiting, A. E. Raftery, Strictly proper scoring rules, prediction, and estimation, Journal of the American Statistical Association 102 (477) (2007) 359–378. doi:10.1198/016214506000001437.
- [39] F. Golestaneh, P. Pinson, H. B. Gooi, Very short-term nonparametric probabilistic forecasting of renewable energy generation - With application to solar energy, IEEE Transactions on Power Systems (2016). doi:10.1109/TPWRS.2015.2502423.
- [40] S. Bentzien, P. Friederichs, Decomposition and graphical portrayal of the quantile score, Quarterly Journal of the Royal Meteorological Society 140 (683) (2014) 1924–1934. doi:10.1002/qj.2284.
- [41] P. Pinson, P. McSharry, H. Madsen, Reliability diagrams for non-parametric density forecasts of continuous variables: Accounting for serial correlation, Quarterly Journal of the Royal Meteorological Society 136 (646) (2010) 77–90. arXiv:arXiv:0801.1618v2, doi:10.1002/qj.559.
- [42] J. Friedman, T. Hastie, R. Tibshirani, Additive logistic regression: A statistical view of boosting (2000). doi:10.1214/aos/1016218223.